

Semiparametric Identification of Wiener Systems Using a Single Harmonic Input and Retrospective Cost Optimization

Anthony M. D'Amato, Bruno O. S. Teixeira, and Dennis S. Bernstein

Abstract—We present a two-step method for identifying SISO Wiener systems. First, using a single harmonic input, we estimate a nonparametric model of the static nonlinearity, which is assumed to be only piecewise continuous. Second, using the identified nonparametric map, we use retrospective cost optimization to identify a parametric model of the linear dynamic system. This method is demonstrated on several examples of increasing complexity.

I. INTRODUCTION

Block-structured models are widely used for system identification [6]. These models provide useful information concerning the dynamic and static components of a system, and thus constitute grey-box models in which the block structure is ascribed physical meaning. The goal of system identification is to model the internal structure of each block from available data.

Among the most widely studied block-structured models are the Wiener [1–4, 8] and Hammerstein [1, 4] models. Each model structure involves a single linear dynamic block and a single nonlinear static block. For these two-block structures, the difficulty of the identification problem typically depends on *a priori* assumptions made about the components, for example, FIR-versus-IIR dynamics, and invertible-versus-noninvertible nonlinearities [8]. Furthermore, identification of Wiener systems is generally considered to be more challenging than identification of Hammerstein systems due to the fact that the input to the nonlinear block is available for Hammerstein systems but not for Wiener systems. In the present paper, we focus on Wiener systems.

The methods for identifying Wiener systems developed in [1, 3] assume that the nonlinear block is invertible. To overcome this requirement, nonparametric probabilistic methods are used in [6]. Alternatively, frequency-domain methods that apply multiple harmonic inputs are employed in [2, 4]. In [4], the multiple harmonic inputs are assigned random phase shifts, and a nonparametric model of the nonlinearity is obtained using the identified linear dynamic model, which is previously estimated in the frequency domain. In [2], the phase shift between the output of the linear dynamic block and the output is exploited in the frequency domain, for each harmonic input.

This work was supported in part by NASA through grants NNX08AB92A and NNX08BA57A, USA, and by FAPEMIG, Brazil.

A. M. D'Amato and D. S. Bernstein are with the Department of Aerospace Engineering, University of Michigan, Ann Arbor, MI, USA. {amdamoto, dsbaero}@umich.edu

B. O. S. Teixeira is with the Department of Electronic Engineering, Federal University of Minas Gerais, Belo Horizonte, MG, Brazil. brunoot@ufmg.br

In the present paper we develop a novel technique for identifying single-input, single-output (SISO) Wiener systems. The proposed approach is semiparametric, which, as described in [6], refers to the fact that the nonlinear block is estimated nonparametrically, whereas the linear dynamics are identified parametrically. To do this, we consider a two-step procedure. In the first step, we apply a single harmonic input signal, and measure the output once the trajectory of the system reaches harmonic steady state. We then examine the output of the system (which is not harmonic due to the nonlinearity) relative to the input, and use the symmetry properties of these signals to estimate the nonharmonic phase shift. This estimate allows us to infer the phase shift of the unmeasured intermediate signal (that is, the output of the linear block) and thus reconstruct this signal up to an arbitrary amplitude. By plotting the output versus the reconstructed intermediate signal, we thus obtain a nonparametric approximation of the nonlinear block of the system.

The second step of the algorithm uses a sufficiently rich signal to estimate the linear dynamics of the system. Since we do not assume that the nonlinear block is invertible, we do not have an estimate of the output of the linear block. To overcome this difficulty, we apply retrospective cost optimization, which uses the available output signal (in this case, the output of the nonlinear block) to recursively update the linear dynamics. This technique is inspired by retrospective-cost-based adaptive control [7], which is used for model updating in [5, 9].

As alluded to above, the two-step identification algorithm described herein does not require invertibility of the nonlinear block as assumed in [1, 3]. In fact, we do not require that the nonlinear block be either one-to-one, onto, or continuous, nor do we assume as in [3] that any specific value of the nonlinearity be known.

II. PROBLEM FORMULATION

Consider the block-structured Wiener model shown in Figure 1a, where \mathcal{L} is the SISO discrete-time linear time-invariant dynamic system

$$x(k+1) = Ax(k) + Bu(k), \quad (1)$$

$$v(k) = Cx(k), \quad (2)$$

with input $u(k) \in \mathbb{R}$ and intermediate signal $v(k) \in \mathbb{R}$, where k is the sample index, and $y(k) \in \mathbb{R}$ is the output

$$y(k) = \mathcal{W}(v(k)), \quad (3)$$

where $\mathcal{W} : \mathbb{R} \mapsto \mathbb{R}$ is the static nonlinearity. We assume that \mathcal{L} is asymptotically stable and \mathcal{W} is piecewise continuous.

Note that we do not assume that \mathcal{W} is invertible, one-to-one, continuous, or (as in [3]) $\mathcal{W}(0) = 0$. Also, we assume that $v(k)$ is not accessible, and that $x(0)$ is unknown and possibly nonzero.

Moreover, Figure 1b shows the scaled-domain modification $\mathcal{W}_\lambda(v) \triangleq \mathcal{W}\left(\frac{v}{\lambda}\right)$ of \mathcal{W} , where λ is a nonzero real number. Therefore, $\mathcal{W}_\lambda(\lambda v) = \mathcal{W}(v)$. Each value of λ scales both the gain of \mathcal{L} and the domain of \mathcal{W} . However, λ is not identifiable.

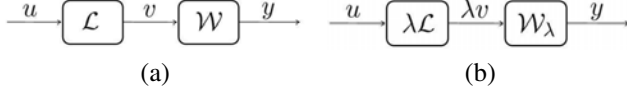


Fig. 1. (a) Block-structured Wiener model, where u is the input, v is the intermediate signal, y is the output, \mathcal{L} is a discrete-time linear time-invariant dynamic system, and \mathcal{W} is a static nonlinearity. (b) An equivalent scaled model, where λ is a scaling factor and \mathcal{W}_λ is a scaled-domain modification of \mathcal{W} satisfying $\mathcal{W}_\lambda(\lambda v) = \mathcal{W}(v)$. The scaling factor λ is not identifiable.

III. NONPARAMETRIC IDENTIFICATION OF THE STATIC NONLINEARITY

Consider the harmonic input signal

$$u(k) = A_0 \sin(\omega_0 k T_s) = A_0 \sin(\Omega_0 k), \quad (4)$$

where A_0 is the amplitude, ω_0 is the angular frequency in rad/sec, T_s is the sample period in sec/sample, and $\Omega_0 \triangleq \omega_0 T_s$ is the angular sample frequency in rad/sample. Since \mathcal{L} is asymptotically stable, it follows that, for large values of k , the intermediate signal v is given approximately by the harmonic steady-state signal

$$v(k) = |G(e^{j\Omega_0})| A_0 \sin(\Omega_0 k + \angle G(e^{j\Omega_0})), \quad (5)$$

where $|G(e^{j\Omega_0})|$ and $\angle G(e^{j\Omega_0})$ are the magnitude and phase shift of the frequency response of $G(\mathbf{z}) = C(\mathbf{z}I - A)^{-1}B$ at the angular sample frequency Ω_0 . Therefore,

$$y(k) = \mathcal{W}(|G(e^{j\Omega_0})| A_0 \sin(\Omega_0 k + \angle G(e^{j\Omega_0}))). \quad (6)$$

Next, note that the continuous-time harmonic signal $\sin(\omega_0 t)$ is symmetric in the intervals $[0, \frac{1}{2}T_0]$ and $[\frac{1}{2}T_0, T_0]$ about the points $\frac{1}{4}T_0$ and $\frac{3}{4}T_0$, respectively, where $T_0 \triangleq \frac{2\pi}{\omega_0}$ is the period of the harmonic input. To preserve symmetry for the sampled signal (4) about the points $\frac{1}{4}T_0$ and $\frac{3}{4}T_0$, we assume that $\Omega_0 = \frac{\pi}{2m}$, where m is a positive integer.

Thus $N_0 \triangleq 4m = \frac{T_0}{T_s}$ is the period of the discrete-time input (4). With this choice of Ω_0 , the sampled signal $u(k)$ is symmetric in the intervals $[0, \frac{1}{2}N_0]$ and $[\frac{1}{2}N_0, N_0]$ about the points $\frac{1}{4}N_0$ and $\frac{3}{4}N_0$, respectively. Furthermore, assuming that $q \triangleq \frac{\angle G(e^{j\Omega_0})}{\Omega_0}$ is an integer, that is, $\frac{\angle G(e^{j\Omega_0})}{\pi}$ is an integer, the intermediate signal $v(k)$, which is shifted relative to $u(k)$ due to $\angle G(e^{j\Omega_0})$, is symmetric about $\frac{1}{4}N_0 + q$ in the interval $[q, \frac{1}{2}N_0 + q]$ and about $\frac{3}{4}N_0 + q$ in the interval $[\frac{1}{2}N_0 + q, N_0 + q]$. If q is not an integer, then $v(k)$ is only approximately symmetric.

Next, we note that the output signal y , which is not generally harmonic, possesses the same symmetry as v on the same intervals. By exploiting knowledge of this symmetry, we can identify the *nonharmonic phase shift* of y relative to u , and thus the phase shift of v relative to u . Since y is not sinusoidal, the nonharmonic phase shift of y relative to u refers to the shifting of the symmetric portions of y relative to the symmetric portions of u . Knowledge of this nonharmonic phase shift allows us to determine v up to a constant multiple, specifically, v is a sinusoid that is shifted relative to u by a known number of samples.

To clarify the above discussion, we present two examples using $A_0 = 1$, $m = 18$ (so that $\Omega_0 = \pi/36$), and $G(\mathbf{z}) = \frac{0.0685}{\mathbf{z} - 0.9164}$. First, consider the polynomial nonlinearity $y = \mathcal{W}(v) = 0.6(v+1)^3 - 1$, which is neither even nor odd. Figure 2a illustrates the resulting signals $u(k)$, $v(k)$, and $y(k)$ in harmonic steady state. Note that u is symmetric about the discrete-time index δ in the interval $[\delta - \frac{1}{4}N_0, \delta + \frac{1}{4}N_0]$ and about $\delta + \frac{1}{2}N_0$ in the interval $[\delta + \frac{1}{4}N_0, \delta + \frac{3}{4}N_0]$. Likewise, v is symmetric about the discrete-time index ε in the interval $[\varepsilon - \frac{1}{4}N_0, \varepsilon + \frac{1}{4}N_0]$ and about $\varepsilon + \frac{1}{2}N_0$ in the interval $[\varepsilon + \frac{1}{4}N_0, \varepsilon + \frac{3}{4}N_0]$. It thus follows that y is symmetric about ε in the interval $[\varepsilon - \frac{1}{4}N_0, \varepsilon + \frac{1}{4}N_0]$ and about $\varepsilon + \frac{1}{2}N_0$ in the interval $[\varepsilon + \frac{1}{4}N_0, \varepsilon + \frac{3}{4}N_0]$.

Second, we consider the even polynomial nonlinearity $y = \mathcal{W}(v) = v^2$. Figure 2b illustrates the resulting signals $u(k)$, $v(k)$, and $y(k)$ in harmonic steady state. The signals u and v are equal to the signals shown in Figure 2a. However, in addition to the two points of symmetry shown in Figure 2a, note that y has two additional points of symmetry, specifically, y is symmetric about $\varepsilon + \frac{1}{4}N_0$ in the interval $[\varepsilon, \varepsilon + \frac{1}{2}N_0]$ and about $\varepsilon + \frac{3}{4}N_0$ in the interval $[\varepsilon + \frac{1}{2}N_0, \varepsilon + N_0]$.

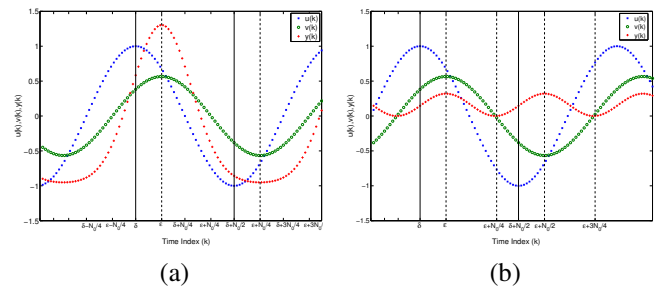
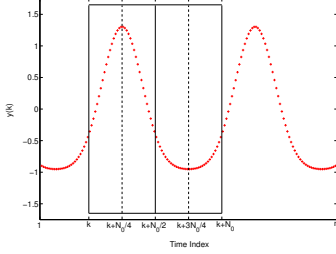


Fig. 2. Illustration of the symmetry properties of the signals u , v , and y given by (4)-(6), respectively, for (a) the non-even polynomial nonlinearity $y = \mathcal{W}(v) = 0.6(v+1)^3 - 1$ and (b) the even polynomial nonlinearity $y = \mathcal{W}(v) = v^2$. The signals u and v are harmonic, whereas y is the output of the nonlinear block \mathcal{W} and thus is not harmonic. Note that, for both cases, u is symmetric about δ in the interval $[\delta - \frac{1}{4}N_0, \delta + \frac{1}{4}N_0]$ and about $\delta + \frac{1}{2}N_0$ in the interval $[\delta + \frac{1}{4}N_0, \delta + \frac{3}{4}N_0]$, while v and y are symmetric about ε in the interval $[\varepsilon - \frac{1}{4}N_0, \varepsilon + \frac{1}{4}N_0]$ and about $\varepsilon + \frac{1}{2}N_0$ in the interval $[\varepsilon + \frac{1}{4}N_0, \varepsilon + \frac{3}{4}N_0]$. In addition, for the case of an even polynomial nonlinearity shown in (b), y is also symmetric about $\varepsilon + \frac{1}{4}N_0$ in the interval $[\varepsilon, \varepsilon + \frac{1}{2}N_0]$ and about $\varepsilon + \frac{3}{4}N_0$ in the interval $[\varepsilon + \frac{1}{2}N_0, \varepsilon + N_0]$.

A. Symmetry Search Algorithm

We now present an algorithm to determine ε from y . We then use ε to estimate the nonharmonic phase shift of y relative to u . For convenience, we assume that the harmonic steady state begins at $k = 0$. Consider the signal y shown in Figure 3, and let $n \geq 6m$ denote the width of the data window so that it includes at least one and a half periods. To encompass a complete signal period, we construct a sliding window with $N_0 + 1$ data points. The window is divided into quarters as shown in Figure 3.



3. Illustration of the symmetry search algorithm. The solid line box comprises the sliding window of length $N_0 + 1$ starting at time k , while the dashed lines indicate the windowed points of symmetry.

Next, for $k = 0, \dots, n - N_0$, define

$$\beta_1(k) \triangleq \sum_{i=1}^{2m-1} |y(k+i-1) - y(k+2m-i+1)|, \quad (7)$$

which is the sum of the absolute difference in magnitude for each pair of candidate symmetric points in the first and second quarters about the point $k + \frac{1}{4}N_0$ for the sliding window starting at time step k . Likewise, for $k = 0, \dots, n - N_0$, define

$$\beta_2(k) \triangleq \sum_{i=1}^{2m-1} |y(k+2m+i-1) - y(k+4m-i+1)|, \quad (8)$$

for each pair of candidate symmetric points in the third and fourth quarters about the point $k + \frac{3}{4}N_0$. The values of β_1 and β_2 quantify the symmetry error about the points $k + \frac{1}{4}N_0$ and $k + \frac{3}{4}N_0$, respectively, for each allowable value of k . Thus, using (7) and (8), we define the *symmetry error index* $\beta(k) \triangleq \beta_1(k) + \beta_2(k)$, corresponding to the sliding window starting at point k , for $k = 0, \dots, n - N_0$.

For $k = 0, \dots, n - N_0$, let $k_0 < N_0$ be the minimizer of $\beta(k)$. We use knowledge of k_0 to determine the location of the points of symmetry ε and $\varepsilon + \frac{1}{2}N_0$ for the sliding window starting at point k_0 . In particular, since k_0 is the starting point of the window that minimizes β and since ε and $\varepsilon + \frac{1}{2}N_0$ are, respectively, the quarter point and three quarter point of the same window, it follows that

$$\varepsilon = k_0 + \frac{1}{4}N_0, \quad \varepsilon + \frac{1}{2}N_0 = k_0 + \frac{3}{4}N_0. \quad (9)$$

Note that, in general, $\beta(k_0) \neq 0$. However if $\frac{\mathcal{L}G(e^{j\Omega_0})}{\pi}$ is an integer, then $\beta(k_0) = 0$, which indicates exact symmetry about $k_0 + \frac{1}{4}N_0$ in the interval $[k_0, k_0 + \frac{1}{2}N_0]$ and about $k_0 + \frac{3}{4}N_0$ in the interval $[k_0 + \frac{1}{2}N_0, k_0 + N_0]$.

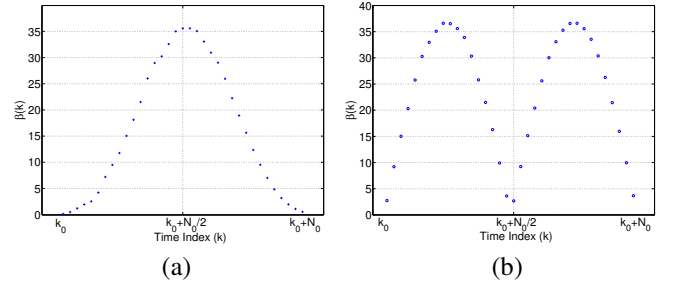
To illustrate the symmetry search algorithm, we reconsider the example considered in Figures 2a and 3, where $y =$

$\mathcal{W}(v) = 0.6(v+1)^3 - 1$. Note that \mathcal{W} is not even. Figure 4a shows the values of β calculated for $y(k)$ on the interval $[k_0, k_0 + 2N_0]$. Since, in Figure 4a, the data window of y is selected to start at $k_0 = \varepsilon - \frac{1}{4}N_0$, the minimum values of $\beta(k)$ occur at k_0 and $k_0 + N_0$, where $k_0 + N_0$ is the start of the next period and, thus, need not be considered. Thus, using the unique minimizer k_0 of $\beta(k)$, it follows that the locations of the points of symmetry are given by (9).

Next, for the even nonlinearity $y = \mathcal{W}(v) = v^2$ considered in Figure 2b, Figure 4b shows the values of $\beta(k)$ calculated for $y(k)$ on the interval $[k_0, k_0 + 2N_0]$. In this case, the minimum values of $\beta(k)$ occur at $k_0, k_0 + \frac{1}{2}N_0$, and $k_0 + N_0$, where $k_0 + N_0$ is the start of the next period and, thus, need not be considered. Thus, using k_0 , it follows that the locations of the points of symmetry are given by (9). Also, using $k_0 + \frac{1}{2}N_0$, we obtain two additional points of symmetry given by

$$\varepsilon + \frac{1}{4}N_0 = k_0 + \frac{1}{2}N_0, \quad \varepsilon + \frac{3}{4}N_0 = k_0 + N_0. \quad (10)$$

This ambiguity is due to the fact that ε and $\varepsilon + \frac{1}{2}N_0$ are the midpoints of two identical symmetric portions of y . Thus, the start of the data window within which the function has the symmetry properties illustrated in Figure 3 can be taken as either k_0 or $k_0 + \frac{1}{2}N_0$. Note that the second minimizer $k_0 + \frac{1}{2}N_0$ appears only for even nonlinearities.



4. Illustration of the symmetry error index $\beta(k)$ given by (7). The values of $\beta(k)$ are shown for two static nonlinearities, namely, (a) a non-even polynomial and (b) an even polynomial.

B. Nonparametric Approximation of the Static Nonlinearity

Using δ , which is assumed to be known from the harmonic input u , and the estimate of ε obtained from y in Section III-A, we now determine an estimate $\hat{\phi}$ of the nonharmonic phase shift of y relative to u by $\hat{\phi} \triangleq \Omega_0(\varepsilon - \delta)$, which is an estimate of $\mathcal{L}G(e^{j\Omega_0})$. Moreover, define the virtual signal

$$\tilde{v}(k) \triangleq A_0 \sin(\Omega_0 k + \hat{\phi}), \quad (11)$$

which is an approximation of the intermediate signal v given by (5) divided by the constant $|G(e^{j\Omega_0})|$. Note that, if $\hat{\phi} = \mathcal{L}G(e^{j\Omega_0})$, then $|G(e^{j\Omega_0})|\tilde{v} = v$. Also, note that the amplitude of $\tilde{v}(k)$ is irrelevant due to the scaling factor λ shown in Figure 1b. Using \tilde{v} and y , the nonparametric estimate of \mathcal{W} is given by

$\hat{\mathcal{W}} \triangleq \{(\tilde{v}(k_0), y(k_0)), (\tilde{v}(k_0 + 1), y(k_0 + 1)), \dots, (\tilde{v}(n), y(n))\}$, (12) where each pair $(\tilde{v}(k), y(k))$, for $k = 0, \dots, n$, determines a value of the nonparametric estimate $\hat{\mathcal{W}}$ of \mathcal{W} .

Figure 4 shows that, depending on the type of nonlinearity, $\beta(k)$ has either one or two minima within each period. For a non-even polynomial nonlinearity, $\beta(k)$ has one minimum within each period. Therefore, the estimate of the nonharmonic phase shift has two candidate values, namely, $\hat{\phi}$ and $\hat{\phi} + \pi$. For an even nonlinearity, $\beta(k)$ has two minima within each period. Therefore, the estimate of the nonharmonic phase shift has four candidate values, namely, $\hat{\phi}$, $\hat{\phi} + \frac{\pi}{2}$, $\hat{\phi} + \pi$, and $\hat{\phi} + \frac{3\pi}{2}$. However, for the even case, $\hat{\phi}$ and $\hat{\phi} + \pi$ yield the same nonparametric model $\hat{\mathcal{W}}$, while $\hat{\phi} + \frac{\pi}{2}$ and $\hat{\phi} + \frac{3\pi}{2}$ yield the same $\hat{\mathcal{W}}$.

Therefore, for both non-even and even cases, there are two candidate nonparametric estimates of \mathcal{W} , both of which are constructed using (11) and (12). The correct nonparametric model will become apparent when identifying the dynamic block of the Wiener system.

IV. PARAMETRIC IDENTIFICATION OF THE LINEAR TIME-INVARIANT DYNAMICS

Using the nonparametric model $\hat{\mathcal{W}}$ of \mathcal{W} , we now identify a model of \mathcal{L} given by $\hat{\mathcal{L}}$ using retrospective cost optimization (RCO) [9]. The RCO algorithm is presented in [5, 9] together with guidelines for choosing its tuning parameters, namely, n_c , p , and α .

Consider the adaptive feedback architecture for $\hat{\mathcal{L}}$ shown in Figure 5, where $\hat{\mathcal{L}}_m$ denotes the initial model with input $w \in \mathbb{R}$ and output $\hat{v} \in \mathbb{R}$, and where $\hat{\mathcal{L}}_\Delta$ denotes the feedback delta model with inputs $u, \hat{v} \in \mathbb{R}$ and output w . The goal is to adaptively tune $\hat{\mathcal{L}}_\Delta$ so that the performance variable

$$z(k) \triangleq y(k) - \hat{y}(k) \quad (13)$$

is minimized in the presence of the identification signal u . For simplicity, we choose $\hat{\mathcal{L}}_m$ to be the one-step delay $1/z$. Together, $\hat{\mathcal{L}}$ and $\hat{\mathcal{W}}$ comprise a *semiparametric model* of the Wiener system.

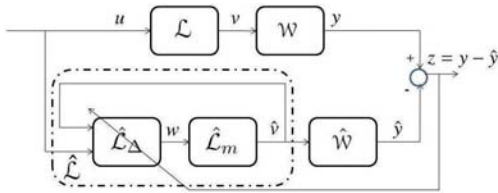


Fig. 5. Identification architecture for Wiener models using RCO.

From Section III-B, recall that there are two candidates for the nonparametric estimate of \mathcal{W} . Thus, we run RCO for each nonparametric estimate of \mathcal{W} and obtain a corresponding parametric model of \mathcal{L} . Note that the performance variable z is calculated for both semiparametric models. We choose the semiparametric model whose performance variable has smaller norm.

An overview of RCO is presented in [5, 9].

V. NUMERICAL EXAMPLES: NOMINAL CASE

To demonstrate semiparametric model identification, we consider various static nonlinearities. For each example, we choose G to have poles $0.34 \pm 0.87j, -0.3141 \pm 0.9j, 0.05 \pm 0.3122j, -0.6875$ and zeros $0.14 \pm 0.97j, -0.12 \pm 0.62j, -0.89$ with monic numerator and denominator. Also, $u(k)$ is chosen to be a realization of zero-mean Gaussian white noise with standard deviation $\sigma_u = 3.5$.

Example 5.1: (Non-even Polynomial) Consider \mathcal{W} defined by

$$y = \mathcal{W}(v) = v^3 + 4v + 7. \quad (14)$$

The parameters for nonparametric identification of \mathcal{W} are $m = 500$ and $A_0 = 5$. Figure 6a compares the true and identified nonlinearities. The RCO parameters used to identify the linear dynamic system are set as $n_c = 9$, $p = 1$, and $\alpha = 1$. Figure 6b shows the frequency response of the true dynamic model G and the identified model using RCO with the identified nonlinearity shown in Figure 6a.

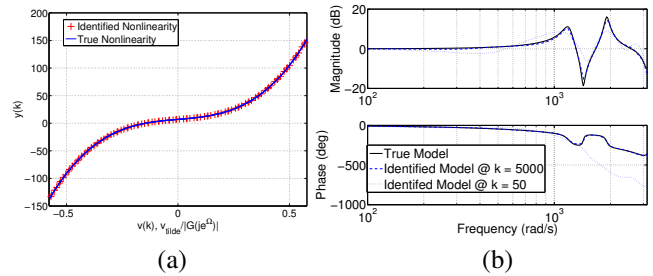


Fig. 6. (a) Identified nonlinearity versus true nonlinearity, where $m = 500$ and $A_0 = 5$. The argument of the identified nonlinearity is scaled by $\frac{1}{|G(e^{j\Omega_0})|}$ to facilitate comparison with the true nonlinearity. (b) Frequency response comparison of the true G and the identified LTI system, where k is the number of data points used to determine the identified model. The RCO controller order is $n_c = 9$ with $p = 1$ and $\alpha = 1$.

Example 5.2: (Even Polynomial) Consider \mathcal{W} defined by

$$y(k) = \mathcal{W}(v) = 7v^4 + v^2. \quad (15)$$

The parameters for nonparametric identification of \mathcal{W} are $m = 500$ and $A_0 = 5$. Figure 7a compares the true and identified nonlinearities. The RCO parameters used to identify the linear dynamic system are set as $n_c = 9$, $p = 1$, and $\alpha = 50$. Figure 7b shows the frequency response of G and the identified model using RCO with the identified nonlinearity shown in Figure 7a.

Next, to illustrate the ambiguity discussed in Section III-B, we select the incorrect nonharmonic phase shift, specifically, $\hat{\phi} + \frac{\pi}{2}$. Figure 8a shows a comparison of the true and identified nonlinearities. Note that the incorrect nonharmonic phase shift produces an erroneous nonparametric model of the nonlinearity. Figure 8b shows a frequency response comparison of G and the model identified using RCO with the identified nonlinearity shown in Figure 8a.

To determine the appropriate phase shift $\hat{\phi}$ or $\hat{\phi} + \frac{\pi}{2}$, we examine the performance variable z given by (13),

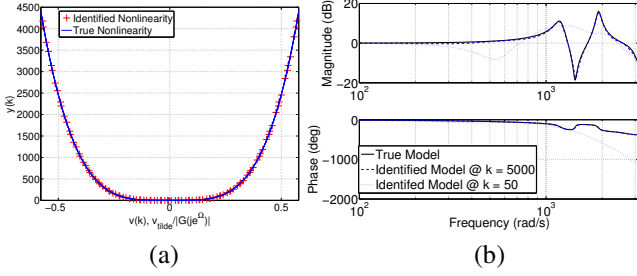


Fig. 7. (a) Identified nonlinearity versus true nonlinearity, where $m = 500$ and $A_0 = 5$. (b) Frequency response comparison of the true G and the identified LTI system, where k is the number of data points used to determine the identified model. The RCO controller order is $n_c = 9$ with $p = 1$, and $\alpha = 50$.

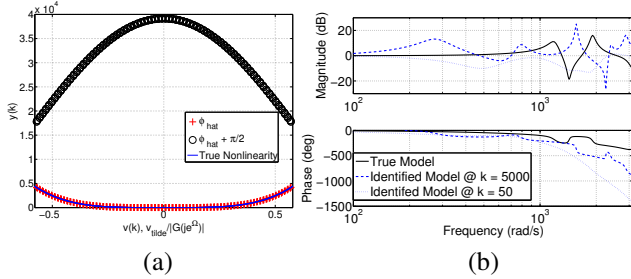
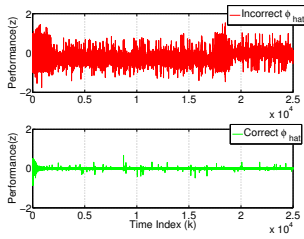


Fig. 8. (a) Identified nonlinearity versus true nonlinearity, where $m = 500$ and $A_0 = 5$. Both candidate values for the nonharmonic phase shift, namely, $\hat{\phi}$ and $\hat{\phi} + \frac{\pi}{2}$, are used to build the two candidate identified nonlinearities. (b) Frequency response comparison of the true G and the identified LTI system, where k is the number of data points used to determine the identified model. The RCO controller order is $n_c = 9$ with $p = 1$, and $\alpha = 50$.



9. Retrospective optimization performance comparison. The upper plot shows the performance variable z for the case in which the nonparametric model is generated using the incorrect candidate for the nonharmonic phase shift $\hat{\phi} + \frac{\pi}{2}$. The lower plot shows z for the case in which the correct candidate $\hat{\phi}$ is used.

which provides insight into which candidate value yields the correct semiparametric model. The upper plot of Figure 9 shows the RCO performance variable z for the incorrect nonparametric model of \mathcal{W} , while the lower plot shows the performance variable for the correct nonparametric model of \mathcal{W} . The correct semiparametric model clearly outperforms the incorrect model.

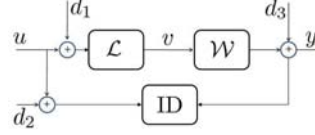
VI. NUMERICAL EXAMPLES: OFF-NOMINAL CASES

We now reconsider the Wiener system (1)-(3) with noise, as shown in Figure 10. The input $u(k)$ is a realization of zero-mean Gaussian white noise with standard deviation $\sigma_u = 3.5$, while $d_1(k) \in \mathbb{R}$ and $d_2(k) \in \mathbb{R}$ are unknown zero-mean Gaussian white disturbances with standard deviations σ_{d_1} and σ_{d_2} , respectively. The output

$$y(k) = \mathcal{W}(v(k)) + d_2(k), \quad (16)$$

has standard deviation σ_y about its mean, and $d_3(k) \in \mathbb{R}$ is an unknown zero-mean Gaussian white disturbance with

standard deviation σ_{d_3} . The disturbance signals $d_1(k)$, $d_2(k)$, and $d_3(k)$ are process, input, and output noise, respectively.



10. Block-structured Wiener model with process, input, and output noise, where d_1 , d_2 , and d_3 are unknown zero-mean Gaussian disturbances.

We now consider additional static nonlinearities, where, for each example, we choose G as in Section V.

Example 6.1: (Deadzone) Consider \mathcal{W} defined by

$$y = \mathcal{W}(v) = \begin{cases} 0, & \text{if } |v| \leq 0.17; \\ v, & \text{if } |v| > 0.17. \end{cases} \quad (17)$$

Furthermore, we consider process and output noise $\sigma_{d_1} = \frac{1}{15}\sigma_u$, $\sigma_{d_3} = \frac{1}{15}\sigma_y$ and $d_2 = 0$. For this problem, the parameters for nonparametric identification are $m = 250$ and $A_0 = 5$. Figure 11a compares the true and identified nonlinearities. The RCO parameters used to identify the linear dynamic system are set as $n_c = 9$, $p = 1$, and $\alpha = 10$. Figure 11b shows the frequency response of G and the identified model using RCO with the identified nonlinearity shown in Figure 11a.

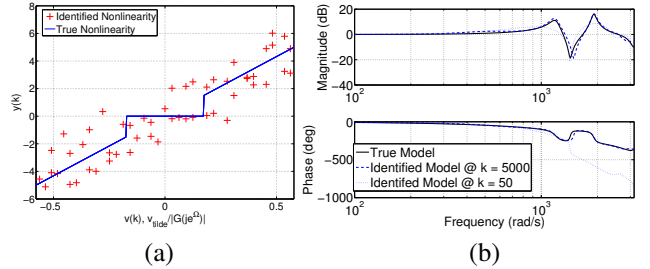


Fig. 11. (a) Identified nonlinearity versus true nonlinearity, where $m = 250$ and $A_0 = 5$. (b) Frequency response comparison of the true G and the identified LTI system, where k is the number of data points used to determine the identified model. The RCO controller order is $n_c = 9$ with $p = 1$ and $\alpha = 10$.

Example 6.2: (Saturation) Consider \mathcal{W} defined by

$$y = \mathcal{W}(v) = \begin{cases} 8.64(v + 0.23) - 3.98, & \text{if } 0.1 < v < 0.4; \\ 1.5, & \text{if } v \geq 0.4; \\ -1.2, & \text{if } v \leq 0.1. \end{cases} \quad (18)$$

Furthermore, we consider input noise $\sigma_{d_1} = \frac{1}{8}\sigma_u$ and $d_2 = d_3 = 0$. The parameters for nonparametric identification are $m = 150$ and $A_0 = 5$. Figure 12a compares the true and identified nonlinearities. The RCO parameters used to identify the linear dynamic system are set as $n_c = 9$, $p = 1$, and $\alpha = 1$. Figure 12b shows the frequency response of G and the identified model using RCO with the identified nonlinearity shown in Figure 12a.

VII. NUMERICAL EXAMPLES: ERROR METRICS

We now investigate the effect of systematically decreasing the amount of available output data that is used to identify the linear block of the Wiener system. Moreover, we investigate the effect of decreasing m , which determines the

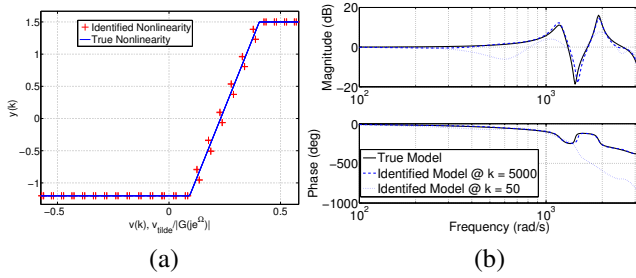


Fig. 12. (a) Identified nonlinearity versus true nonlinearity, where $m = 150$ and $A_0 = 5$. (b) Frequency response comparison of the true G and the identified LTI system, where k is the number of data points used to determine the identified model. The RCO controller order is $n_c = 9$ with $p = 1$ and $\alpha = 1$.

number of points in the nonparametric model, and therefore affects the fidelity of $\hat{\mathcal{W}}$.

To quantify the accuracy of the identified semiparametric model, we compute the root-mean-square error (RMSE) for the first 15 Markov parameters of the true linear system and the identified linear system. The linear model is the same as in Sections V and VI, while \mathcal{W} is given by (14).

A. Effect of Disturbances

To evaluate the effect of σ_{d_1} , σ_{d_2} , and σ_{d_3} , we decrease the number of available data points from 4000 to 10. For each case, we perform a 100-run Monte Carlo simulation with a signal-to-noise ratio of 10. We consider the effect of d_1 , d_2 , and d_3 individually, as well as the effect of all three noise signals, which may be uncorrelated or correlated. Furthermore we consider when d_1 and d_3 are correlated, and d_2 and d_3 are correlated.

Figure 13 demonstrates the increase in error for decreasing amounts of available data. Furthermore, we see that the cases with correlated disturbances yield similar results compared to the case with uncorrelated disturbances.

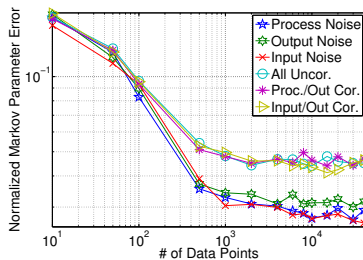


Fig. 13. RMSE Markov parameter error versus number of data points. For each number of data points we perform a 100-run Monte Carlo simulation.

B. Nonparametric Model Accuracy

We now perform a Monte Carlo simulation to evaluate how m affects the accuracy of the identified linear system. Specifically, we vary m from 1 to 100. For each value of m we average the result over 100 simulations. We consider the nominal case, that is, without noise.

Figure 14 shows that RMSE generally decreases as m increases. Note that, for this example, only a slight decrease in RMSE is observed for $m \geq 20$.

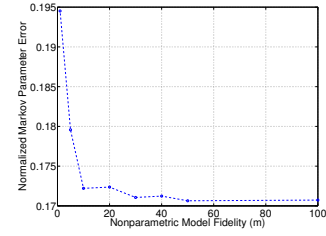


Fig. 14. RMSE Markov parameter error for an increasing number of points in the nonparametric model. For each value of m , a 100-run Monte Carlo simulation is performed.

VIII. CONCLUSIONS

In this paper we develop a two-step method to identify semiparametric models for SISO discrete-time Wiener systems. We make two assumptions, namely, the linear dynamic block is asymptotically stable, and the static nonlinearity is piecewise continuous.

First, we choose a single harmonic input and measure the system output when the state trajectory is in harmonic steady state. By exploiting symmetry properties of these signals, we approximate the nonharmonic phase shift and, therefore, estimate the intermediate signal. Using the estimate of the intermediate signal, a nonparametric model of the static nonlinearity is obtained.

Second, using the identified nonparametric model, we use retrospective cost optimization to identify a parametric model of the dynamic system. In fact, the nonparametric model used with RCO can be obtained using any method.

This method is effectively demonstrated on several examples of increasing complexity, including nonlinearities in the form of both even and non-even polynomials, deadzone, and saturation, and disturbances on the form of process, input, and output noise.

REFERENCES

- [1] L. A. Aguirre, M. C. S. Coelho, and M. V. Corrêa. On the Interpretation and Practice of Dynamical Differences between Hammerstein and Wiener Models. *IEE Proc. - Control Theory Appl.*, v. 152, n. 4, pp. 349–356, 2005.
- [2] E. W. Bai. Frequency Domain Identification of Wiener Models. *Automatica*, v. 39, n. 9, pp. 1521–1530, 2003.
- [3] E. W. Bai and J. Reyland. Towards Identification of Wiener Systems with the Least Amount of *a Priori* Information: IIR cases. *Automatica*, v. 45, pp. 956–964 2009.
- [4] P. Crama and J. Schoukens. Initial Estimates of Wiener and Hammerstein Systems Using Multisine Excitation. *IEEE Trans. Instrum. Meas.*, v. 50, n. 6, pp. 1791–1795, 2001.
- [5] A. M. D’Amato and D. S. Bernstein. LFT Identification Using Retrospective Cost Optimization. *Proc. SYSID*, pp. 450–455, Saint-Malo, France, July 2009.
- [6] W. Greblicki and M. Pawlak. *Nonparametric System Identification*, Cambridge University Press, 2008.
- [7] J. B. Hoagg, M. A. Santillo, and D. S. Bernstein. Discrete-Time Adaptive Command Following and Disturbance Rejection for Minimum Phase Systems with Unknown Exogenous Dynamics. *IEEE Trans. Autom. Contr.*, v. 53, n. 4, pp. 912–928, 2008.
- [8] S. Lacy and D. S. Bernstein. Identification of FIR Wiener Systems with Unknown, Non-invertible, Polynomial Nonlinearities. *Int. J. Control*, v. 76, pp. 1500–1507, 2003.
- [9] M. A. Santillo, A. M. D’Amato, and D. S. Bernstein. System Identification Using a Retrospective Correction Filter for Adaptive Feedback Model Updating. *Proc. ACC 2009*, pp. 4392–4397, St. Louis, MO, June, 2009.